Wiles and wanderings: immune-evasive maneuvers of skin-penetrating parasites

Winkel, B.M.F.

6
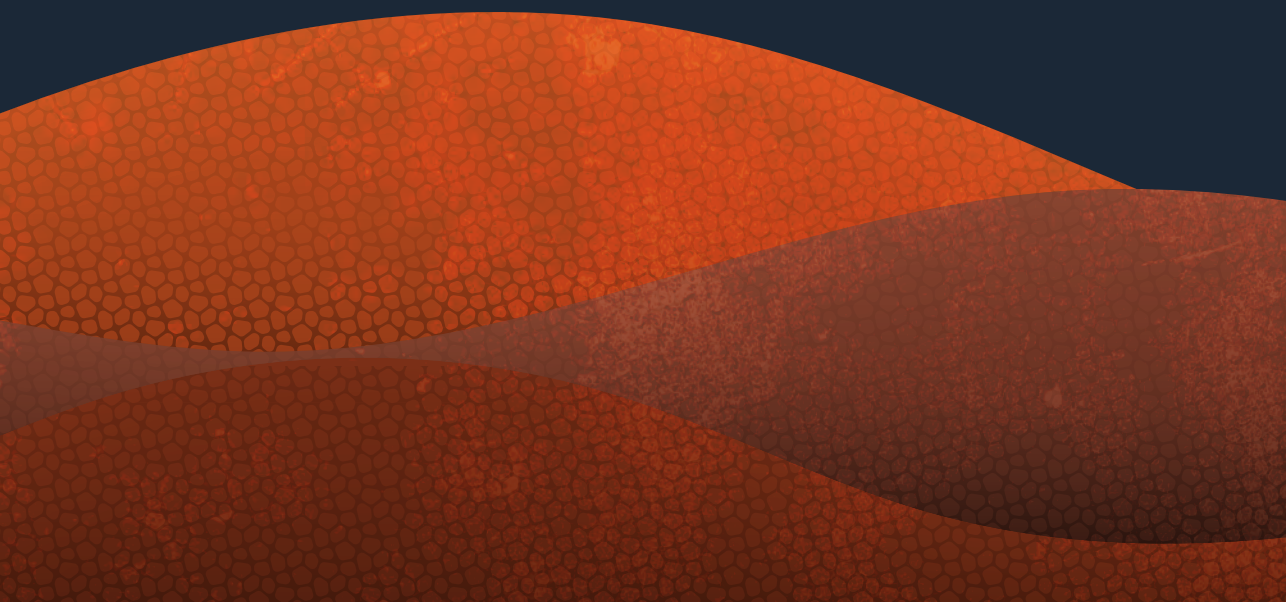
A tracer-based method enables tracking of *Plasmodium falciparum* malaria parasites during human skin infection

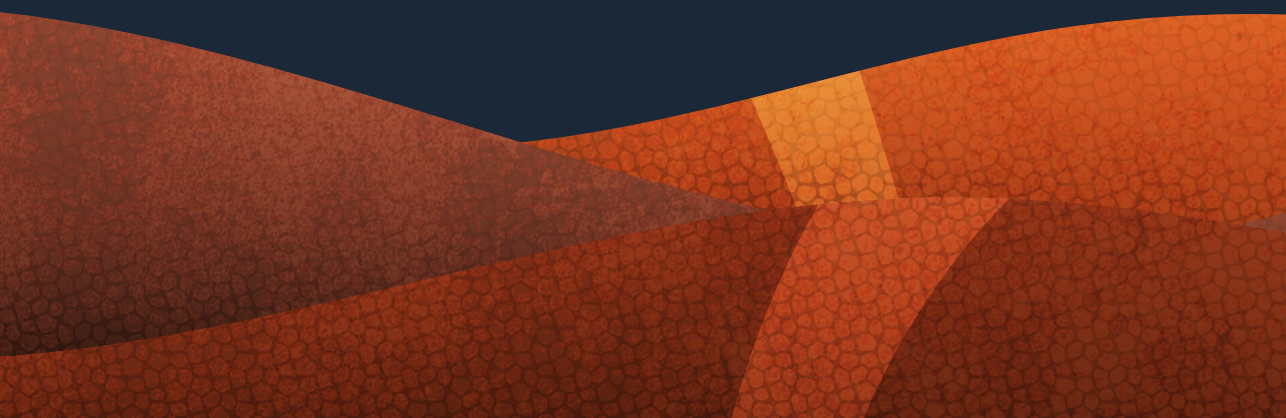Béatrice M.F. Winkel, Clarize M. de Korne, Matthias N. van Oosterom, Diego Staphorst, Anton Bunschoten, Marijke C.C. Langenberg, Séverine C. Chevalley-Maurel, Chris J. Janse, Blandine Franke-Fayard, Fijs W.B. van Leeuwen, Meta Roestenberg

ABSTRACT

Introduction: The skin stage of malaria is a vital and vulnerable migratory life stage of the parasite. It has been characterized in rodent models, but remains wholly uninvestigated for human malaria parasites. To enable in depth analysis of not genetically modified (non-GMO) *Plasmodium falciparum* (*Pf*) sporozoite behavior in human skin, we devised a labelling technology (Cy5M$_2$, targeting the sporozoite mitochondrion) that supports tracking of individual non-GMO sporozoites in human skin.

Methods: Sporozoite labelling with Cy5M$_2$ was performed *in vitro* as well as via the feed of infected Anopheles mosquitos. Labelling was validated using confocal microscopy and flow cytometry and the fitness of labelled sporozoites was determined by analysis of infectivity to human hepatocytes *in vitro*, and *in vivo* in a rodent infection model. Using confocal video microscopy and custom software, single-sporozoite tracking studies in human skin-explants were performed.

Results: Both *in vitro* and in mosquito labelling strategies yielded brightly fluorescent sporozoites of three different *Plasmodium* species. Cy5M$_2$ uptake colocalized with MitoTracker® green and could be blocked using the known Translocator protein (TSPO)-inhibitor PK11195. This method supported the visualization and subsequent quantitative analysis of the migration patterns of individual non-GMO Pf sporozoites in human skin and did not affect the fitness of sporozoites.

Conclusions: The ability to label and image non-GMO *Plasmodium* sporozoites provides the basis for detailed studies on the human skin stage of malaria with potential for *in vivo* translation. As such, it is an important tool for development of vaccines based on attenuated sporozoites and their route of administration.

Keywords: malaria, sporozoites, skin, molecular Imaging, cell tracking.

Graphical Abstract

Mitochondria of malaria sporozoites can be labelled *in vitro* or within mosquito glands using Cy5M$_2$. Using custom software, labelled non-GMO *Pf* sporozoites are tracked and their migration is studied in human skin.
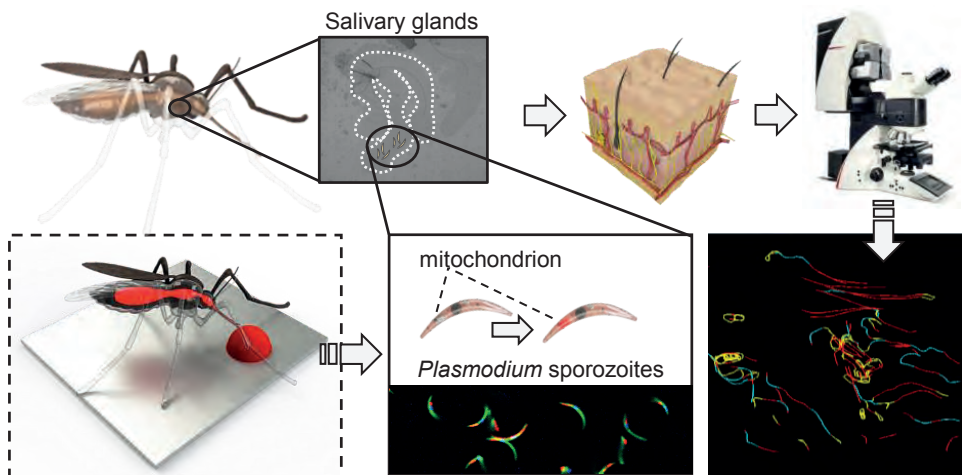
INTRODUCTION

Despite global control efforts, malaria remains the most deadly parasitic disease worldwide accounting for 435.000 deaths in 2017 alone[1], particularly among children below 5 years of age in Sub-Saharan Africa. Decades of research into malaria vaccine development has led to a focus on immune recognition of the clinically silent pre-erythrocytic stage of *Plasmodium* parasites, i.e. sporozoites injected by an infected mosquito that infect liver cells. At this stage, the number of parasites is still low (~100 sporozoites are injected per mosquito bite[2]) and during their migration from the skin inoculation site to the liver the extracellular sporozoites are vulnerable to attack by immunoglobulins[3,4]. Ultimately, only around a quarter of injected sporozoites will make their way from the injection site to the liver, leaving the majority behind in the skin[5].

Pre-erythrocytic immunity to malaria can be induced by repeated exposure to attenuated *Plasmodium falciparum* (*Pf*) sporozoites that arrest development in the liver[6]. Remarkably, these sporozoites induce a strong protective immune response when delivered by the bite of *Pf* infected mosquitoes[2,6] or following intravenous (IV)

administration of purified attenuated *Pf* parasites[7,8] , but intradermal (ID) syringe injection of the latter yields inferior protective immunity both in human and in rodent models of malaria[7,9,10]. However, the use of live mosquitoes or IV administration for large scale vaccination in sub-Saharan countries is not practical.

To rationally design a highly potent malaria vaccine that helps trigger immunity at the pre-erythrocytic stage, more insight into the skin-liver migration mechanisms and immune priming by sporozoites is urgently needed. In rodents, genetically engineered murine *Plasmodium* parasites expressing reporter proteins such as green fluorescent protein (GFP) or luciferase provided unprecedented insight into host-to-host parasite transmission and subsequent migratory behavior of sporozoites from skin to liver. With the use of such tools, sporozoite motility in the skin was visualized[11-13] and the initial dermal immunological responses to injected parasites could be characterized[14,15]. The clinical translation of these rodent malaria characteristics poses some challenges: 1) the difference between rodent and human skin in anatomy and the population of skin-resident immune cells makes it difficult to translate rodent data to humans, and 2) application of transgenic reporter parasites in humans is undesirable. As a consequence, there is demand for imaging technologies that support tracking of single not genetically modified (non-GMO) *Pf* sporozoites in human skin.

Molecular imaging provides a means to monitor the location of pathology *in vivo*[16]. While this technology is most advanced in oncological settings, it also proved to be of value for the detection of infectious diseases, particularly in bacterial infections[17]. Uniquely, many imaging modalities and targets in biomedical imaging are universal. Exogenous fluorescent tracers are not only standard tools in biomedical *in vitro* assays, but are also increasingly clinically employed to provide high resolution real-time guidance during interventions e.g. for skin cancers[18]. Based on these utilities, we reasoned fluorescent tracers could also be used to track non-GMO sporozoites in human skin.

We investigated the receptor specific uptake of the mitochondrial Cy5-methyl-methyl ($Cy5M_2$) tracer. Based on the chemical properties of $Cy5M_2$: lipophilicity and charge, as well as structure, we hypothesized that translocator proteins (TSPO), formally known as the peripheral-type benzodiazepine receptor (PBR), at the outer mitochondrial membrane[19,20] could be a potential target of this tracer. We demonstrate $Cy5M_2$ mitochondrial labelling capacity of sporozoites which can be blocked by the known TSPO inhibitor PK1119521. $Cy5M_2$ enables labelling of multiple *Plasmodium* species, both *in vitro* and in the mosquito host. Additionally, we studied the cell-tracking

utility of Cy5M$_2$-labelled *Pf* sporozoites in a human skin explant model. As a proof of concept for their future use, the fitness of Cy5M$_2$-labelled sporozoites was studied in an *in vitro* human hepatocyte infection assay as well as *in vivo* in a rodent infection model.

MATERIALS AND METHODS

Parasites and animals

Sporozoites were obtained from two rodent malaria species *Plasmodium berghei* (*Pb*) and *Plasmodium yoelli* (*Py*). We used the following wild type and transgenic lines that express fluorescent and/or luminescent reporter proteins: Wild type *Pb* ANKA (cl15cy122); *Pb* line 1868cl1 expressing mCherry and luciferase under the constitutive HSP70 and eef1a promotors respectively[23] (RMgm-1320, www.pberghei.eu) *Pb* line Bergreen[24], Wild type *Py* 17XNL (RMgm-688, www.pberghei.eu22); *Py* line 1971cl125 expressing green fluorescent protein (GFP) and luciferase under the constitutive eef1a promoter (RMgm-689, www.pberghei.eu). Mosquitoes were infected by feeding on infected mice as described previously[26]. For all experiments we used female Swiss mice (6-7 weeks old; Charles River, Leiden, The Netherlands). In addition, sporozoites were obtained from the human parasite *Pf* (NF5427, kindly provided by Radboudumc, Nijmegen, The Netherlands). Mosquitoes were infected by standard membrane feeding as previously described[28].

All animal experiments of this study were approved by the Animal Experiments Committee of the Leiden University Medical Center (DEC 14307). The Dutch Experiments on Animal Act is established under European guidelines (EU directive no. 86/609/EEC regarding the Protection of Animals used for Experimental and Other Scientific Purposes). All experiments were performed in accordance with relevant guidelines and regulations.

In vitro Cy5M2 labelling of sporozoites

Salivary glands from infected mosquitoes were dissected manually at day 14-21 (*Py* and *Pf*) or day 21-28 post infection (*Pb*). Glands were incubated in RPMI 1640 (Invitrogen, Carlsbad, CA, USA) supplemented with 10% heat inactivated Fetal Calf Serum (FCS; Bodinco, Alkmaar, The Netherlands) containing 2,6µM Cy5-methyl-methyl (Cy5M2; 1ug/ml; for compound details see supporting information; Figure S1) or, 100nM MitoTracker® Green for 30 minutes at 28°C or mock stained using RPMI 10% FCS only. TSPO blocking experiments were performed by incubating sporozoites with the known TSPO inhibitor PK11195 21 (50 µM; 40 minutes at 37˚C; see supporting information) before the incubation with Cy5M2. Subsequently, salivary glands were washed twice in RPMI

10% FCS and either imaged directly, or homogenized and filtered over a 40μm filter (Falcon, Corning, Amsterdam, The Netherlands). The whole salivary gland, or solution containing sporozoites was pipetted onto a microscopy slide for live imaging using either a confocal (Leica TCS SP8, Wetzlar, Germany, 40x objective) or a conventional fluorescence microscope (Leica AF6000LX, Wetzlar, Germany, 40x objective). Nuclei were counterstained with Hoechst 33342 10 minutes before imaging.

In vivo Cy5M$_2$ labelling of sporozoites

Mosquitoes were infected either with wild type (WT) or transgenic *Pb* or *Py*. In addition, mosquitoes were infected with WT *Pf* as previously described[28]. Infected mosquitoes were fed on fresh whole blood or 5% glucose in water containing 26μM Cy5M2 (10μg/ml) at day 21-28 (*Pb*) or day 14-21 post infection (*Py* and *Pf*). Feeding was performed using water-heated, glass mosquito feeders at 39°C as previously described[28], in an interrupted feeding schedule of five times two minutes. To maximize feeding behavior, we withheld glucose 24 hours prior to feeding. Immediately after feeding, salivary glands of fed mosquitoes were dissected and placed on a microscopy slide for imaging. Nuclei were counterstained *in vitro* using Hoechst 33342. Slides were imaged using a Leica TCS SP8 confocal microscope with a 40x objective.

Flow Cytometry

Salivary glands containing GFP expressing *Pb* (Bergreen) sporozoites were labelled with Cy5M$_2$ using either the *in vitro* or the *in vivo* labelling technique (see above) or mock stained *in vitro*. Glands were homogenized, stained with Hoechst 33342 *in vitro*, and resuspended in FACS (Flow Cytometric Cell Sorting) buffer (Phosphate-buffered saline (PBS; Braun, Melsungen, Germany) containing 2mM Ultra-pure EDTA (Invitrogen, Carlsbad CA, USA) and 0.5% Bovine serum albumin; BSA (Roche, Basel, Switzerland)). Samples were measured by LSR FortessaTM (BD Bioscience, Franklin Lakes, NJ, USA) and analyzed in FlowJoTM version 9.9.5 (FlowJo LLC, Ashland, OR, USA). Sporozoites were selected by gating on GFP-positive events and Cy5M2 fluorescence signal was quantified in Median Fluorescent Intensity (MFI). Events were normalized to FlowJo algorithms (% of max) to account for the differences in numbers of sporozoites measured per sample.

In vitro sporozoite fitness assay

Sporozoite fitness after labelling was established by measuring *in vitro* infection of hepatocytes and development within hepatocytes as described previously[29]. In brief, 5x104 *Pb* sporozoites of line 1868cl1 expressing mCherry were stained *in vitro* with Cy5M$_2$ or mock stained as described above. Sporozoites were incubated with cells of a HUH7 human hepatoma cell line in a 1:1 ratio in RPMI 10% FCS at 37 degrees for 44

hours. Hepatoma nuclei were stained using Hoechst 33342. Live imaging of liver stage parasite development (presence of liver schizonts) was performed using a conventional fluorescent microscope (Leica AF6000LX). In addition, infectivity was quantified by real-time PCR. DNA was isolated from infected cells 4 hours post infection using a QIAamp DNA Mini Kit (Qiagen, Hilden, Germany) and a real-time PCR was performed as previously described using a cross-species 18S gene based cross species *Plasmodium* probe[30].

In vivo sporozoite fitness assay

Sporozoite fitness after labelling was established by measuring parasite liver loads *in vivo* after infection of mice with labelled parasites. Whole salivary glands of mosquitoes infected with *Pb* line 1868cl1 were collected in RPMI medium and stained with $Cy5M_2$ *in vitro* or mock stained in medium as described above. Sporozoites were isolated as described above (section *In vitro* $Cy5M_2$ labelling of sporozoites). The free sporozoites were counted in a Bürker counting chamber using phase-contrast microscopy. A total number of 5x104 sporozoites was administered to mice by ID injection of 10 µl at both upper thighs using a 30G x 8 mm needle (BD Micro-Fine, BD Biosciences, Breda, The Netherlands). Prior to administration of sporozoites, mice were anesthetized using the isoflurane-anesthesia system (XGI-8, Caliper Life Sciences, Waltham, MA, USA) and shaved in order to optimize the precision of administration.

Parasite liver loads were determined in live mice at 44 hours post infection by real time *in vivo* imaging of luciferase-expressing liver stages as previously described[31]. Liver stages were visualized by measuring luciferase activity of parasites in whole bodies of anesthetized mice using the IVIS Lumina II Imaging System (Perkin Elmer Life Sciences, Waltham, MA, USA). D-luciferin was dissolved in PBS (100 mg/kg; Caliper Life Sciences) and injected subcutaneously in the neck. Animals were kept anesthetized during the measurements, which were performed within 8 minutes after the injection of D-luciferin. Quantitative analysis of bioluminescence of whole bodies was performed by measuring the luminescence signal intensity using the ROI (region of interest) settings of the Living Image® 4.4 software (Perkin Elmer Life Sciences). Presence of blood parasitemia and prepatent period was determined by Giemsa-stained blood smear at day 4 to 10 post sporozoite infection. The prepatent period (measured in days post sporozoite infection; prepatency) ends at the day that blood stage infection with 0.5-2% parasitemia is observed.

Imaging of *Pf* sporozoites in human skin explants

Human skin explants were obtained from patients undergoing abdominal reduction surgery (CME approval number: B18-009). Immediately after surgery, skin explants

were injected intradermally with 106 *in vitro* Cy5M$_2$-labelled *Pf* sporozoites. Sporozoites were mixed with Yellow-Green fluorescent 500nm Latex nanoparticles (Sigma Aldrich) in order to locate the injection site microscopically. A 6mm punch biopsy was taken at the injection site. Biopsies were sliced longitudinally through the injection site and mounted on a microscopy slide with a 1 mm depression in RPMI 10% FCS. Slides were imaged for 30-60 consecutive minutes using a Leica TSC SP8 Confocal microscope with accompanying Leica LASX software, using an exposure time of approximately 1.7 seconds per frame and a 40x objective. Recorded microscopy movies were analyzed for sporozoite motility, using a custom MATLAB software (The MathWorks Inc. Natick, MA, USA) termed SMOOT$_{\text{human skin}}$. In this application tailored software package, sporozoite locations were segmented per movie frame, based on both fluorescence intensity and shape. To reconstruct sporozoite movement over time, median pixel locations per segmented sporozoite shape were connected in time, based on both pixel and frame locations. Based on the dynamic behavior of the sporozoites it was possible to i.a. isolate the following features: migration pattern, speed and parameters of track tortuosity (see supporting information for more detail). SMOOT$_{\text{human skin}}$ software can be made available upon request.

RESULTS

In vitro labelling of sporozoites with Cy5M$_2$

Salivary glands of mosquitoes containing GFP-expressing *Plasmodium berghei* (*Pb*) sporozoites were incubated with Cy5M$_2$ to achieve labelling of sporozoite mitochondria *in vitro*. Confocal microscopy of salivary sporozoites revealed a single fluorescent spot adjacent to the nucleus, in agreement with the presence of single parasite mitochondrion (Figure 1A)[32,33]. The universal applicability of this *in vitro* labelling technique for sporozoites of different *Plasmodium* species was demonstrated by labelling murine *Plasmodium yoelii* (*Py*) and *Pb* and human *Pf* sporozoites (Supporting information; Supplementary figure S2). Cy5M$_2$ uptake by sporozoites was quantified by flow cytometry, which showed a 430-fold increase in median fluorescence intensity (MFI) of Cy5M$_2$ labelled parasites (Cy5M$_2$ MFI of 7493) compared to unlabeled controls (Cy5M$_2$ MFI of 17.5; Figure 1B). All sporozoites exposed to Cy5M$_2$ showed tracer uptake, however, a small proportion of sporozoites (8.47%) take up Cy5M$_2$ less readily, as reflected by their lower mean fluorescent intensity (Figure 1B).
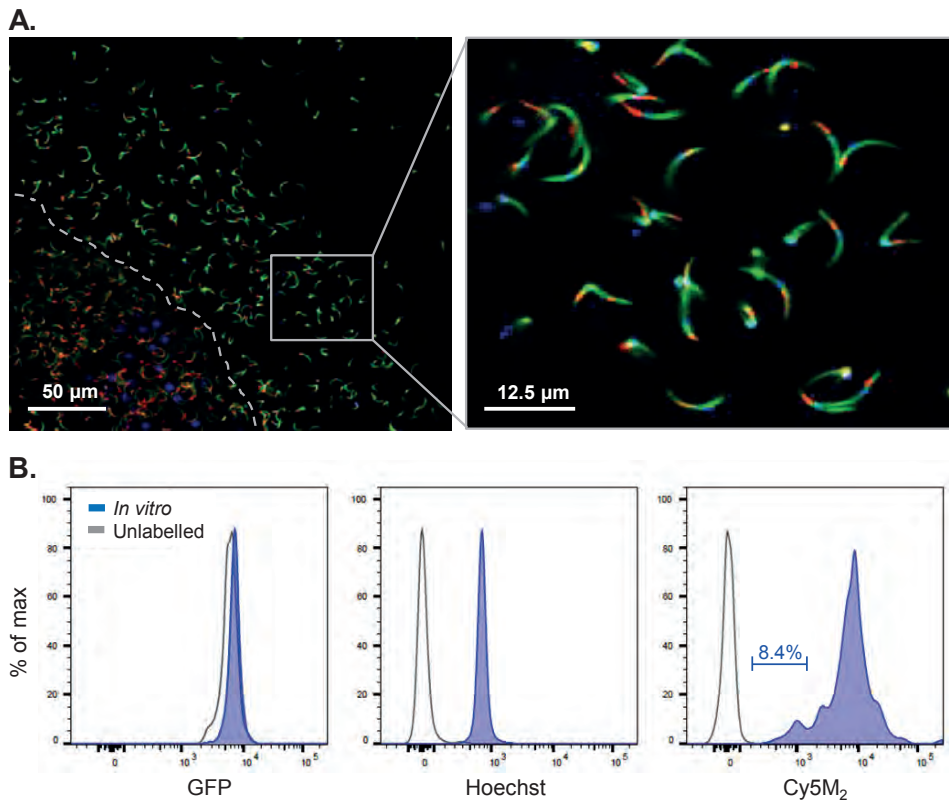
A.

B.

Figure 1. Cy5M labels sporozoites *in vitro*. (**A**) Fluorescence-microscopy analysis of *In vitro labelled Pb* sporozoites (Bergreen) expressing GFP (green; cytoplasmic) and a single spot Cy5M (red). Parasite nuclei are stained with Hoechst (blue). Dotted line demarcates the salivary gland edge, separating expelled sporozoites from gland sporozoites. (**B**) Quantification of fluorescence by Flow Cytometry. Gray lines represent background signal in unlabeled sporozoites. Blue lines show signal after labelling with Hoechst and $Cy5M_2$. All sporozoites are GFP^+. Fluorescence intensity on x-axis, Events normalized using FlowJo algorithms in order to account for the differences in numbers of sporozoites measured per sample (% of max; y-axis).

Co-staining with MitoTracker® green confirmed $Cy5M_2$ labelling was restricted to the mitochondrion (Figure 2A; Supporting information Supplementary figure S3). In line with our assumptions that mitochondrial TSPO could be a potential target of $Cy5M_2$, competition with the known TSPO inhibitor PK11195 reduced the mitochondrial uptake in a breast cancer cell line (X4-cells), schwannoma cell line (RT4-D6P2T; Supplementary figure S4) as well as directly in *Pb* sporozoites (Figure 2B).
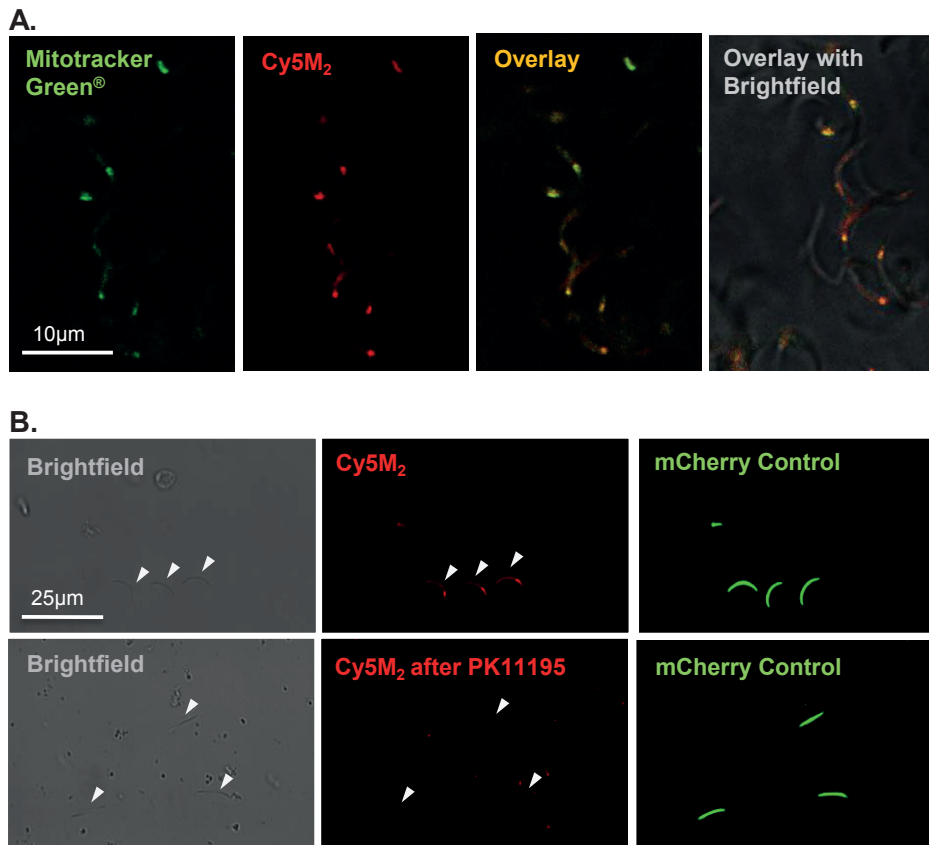
A.

B.

Figure 2. Cy5M$_2$ labels sporozoite mitochondria and can be blocked by TSPO inhibitor PK11195. (**A**) Double staining of Cy5M$_2$ (red) with Mitotracker® green (green) shows mitochondrial staining in labelled *Pb* sporozoites. (**B**) Cy5M$_2$ (red) labelling in mCherry expressing (green) sporozoites can be blocked by addition of the known TSPO inhibitor PK1119.

Labeling of sporozoites with Cy5M$_2$ in mosquitoes

Infected mosquitoes containing salivary gland sporozoites were exposed to Cy5M$_2$ by membrane feeding. As a result of the tracer's molecular size (383,25 Mw) it rapidly diffused through the mosquito to label sporozoites within salivary glands (Figure 3). In order to study the tracer distribution throughout highly auto fluorescent mosquitoes, we collected midguts and salivary glands of Cy5M$_2$ fed mosquitoes and imaged those organs separately. This indicated universal staining of mosquito organs, including the salivary glands and gland residing sporozoites (Figure 3, Supplementary figure S5). Quantification of the *in vivo* tracer uptake in sporozoites by flow cytometry revealed
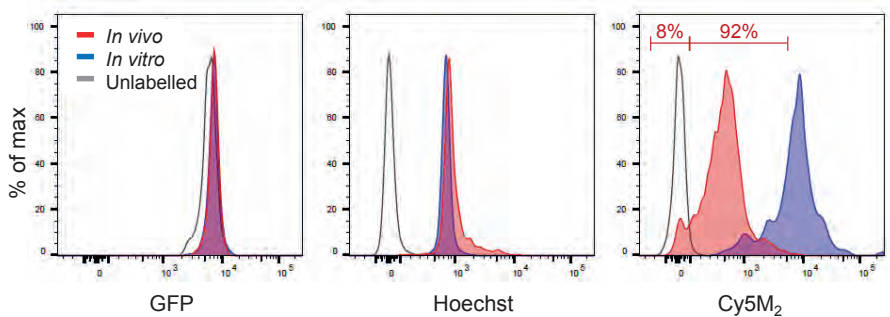
A.
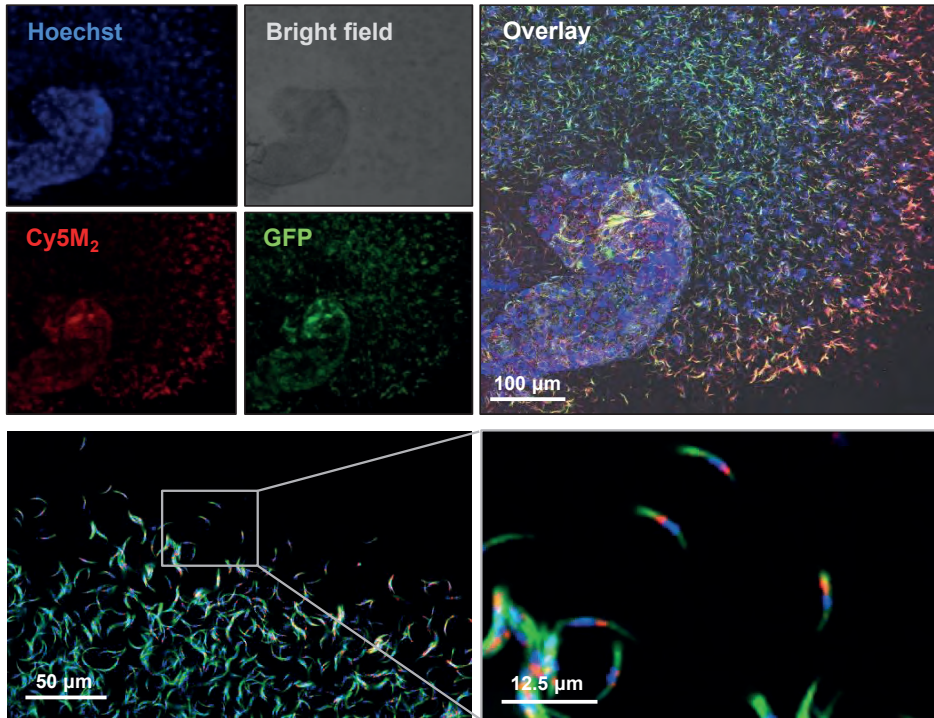
B.

Figure 3. Feeding infected mosquitoes on blood containing Cy5M[2] labels sporozoites. (**A**) Fluorescence-microscopy analysis showing a whole salivary gland with a cloud of expelled, *in vivo* Cy5M[2] (red) labelled, GFP expressing (green) *Pb* sporozoites. Nuclei are stained with Hoechst (blue). Scale bar 100 μM. Below: magnification shows mitochondrial staining. (**B**) Flow Cytometric quantification shows a 30 fold increase in fluorescence in 92% of mosquito-fed sporozoites (*in vivo*, red) compared to unlabeled controls (grey line). Highest uptake was seen with *in vitro* labelled parasites (blue). Fluorescence intensity on x-axis. Events are normalized using FlowJo algorithms in order to account for the differences in numbers of sporozoites measured per sample (% of max; y-axis).

clear fluorescence uptake by 92% of sporozoites and a 30-fold increase of $Cy5M_2$ MFI compared to unlabeled control sporozoites (Figure 3B; $Cy5M_2$ MFI of labelled sporozoites was 515 compared to 17.5 of unlabeled controls).
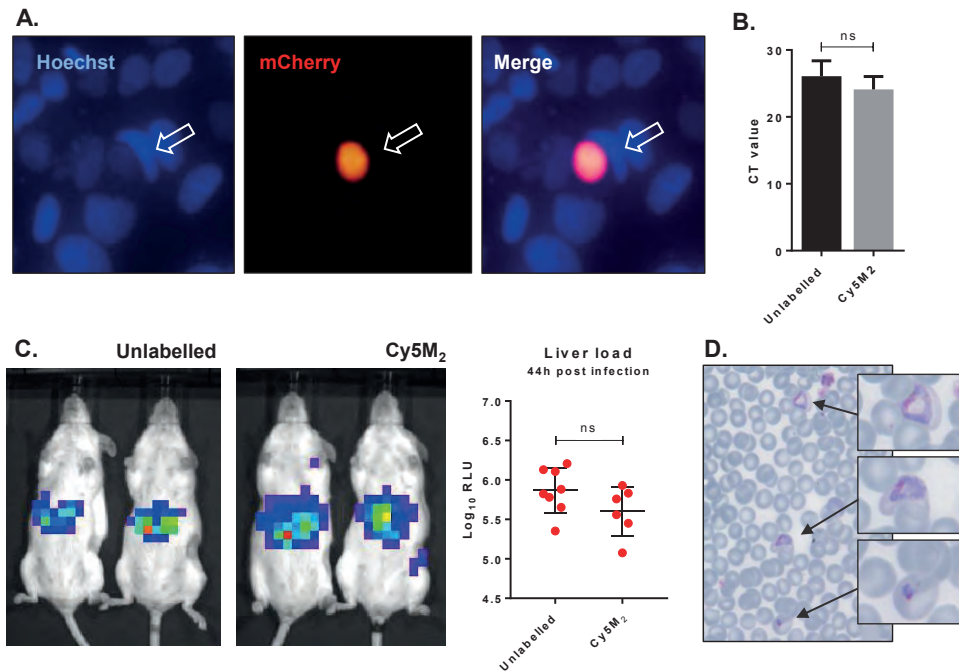

Figure 4. Labelled sporozoites retain their infectivity *in vitro* and *in vivo*. (**A**) Human hepatoma (HUH7) cell line infection with *in vitro* $Cy5M_2$ labelled, mCherry expressing *Pb* sporozoites shows liver schizont (arrow) formation at 44h post infection. (**B**) PCR data showing similar levels of HUH7 cell infection with $Cy5M_2$ labelled sporozoites compared to unlabeled controls. (p=0.52) (**C**) Representative IVIS Lumina image of Swiss mice injected with luciferase expressing sporozoites. Mice injected with *in vitro* $Cy5M_2$ labelled *Pb* (right panel*)* show similar liver load 44h post injection compared to mice injected with mock labelled controls (left panel). Quantification of liver loads in relative light units (RLU), pooled data of two experiments. Eight mice per group. p=0,18 (**D**) Representative blood smear at day 7 post infection with $Cy5M_2$ labelled *Pb* shows blood stage malaria.

Fitness of $Cy5M_2$ labelled sporozoites.

The fitness of $Cy5M_2$ labelled sporozoites was first analyzed by determination of *in vitro* infectivity of mCherry-expressing *Pb* sporozoites to human Huh7 hepatoma cells. As $Cy5M_2$ is lost during liver stage development of parasites, we detected fully mature liver stages using mCherry expression at 44 hours after infection. Figure 4A shows a

liver schizont, demonstrating that labelled sporozoites are able to infect hepatocytes and develop into mature forms. Quantification of *Pb* DNA within Huh7 monolayers by reverse transcriptase-polymerase chain reaction (RT-PCR) showed comparable levels of invasion of hepatocytes and development into liver-schizonts in cells infected with labelled versus unlabeled sporozoites (p=0.52); Figure 4B).

Next we analyzed sporozoite fitness *in vivo* by determination of parasite liver loads in mice infected with labelled *Pb* sporozoites. Parasite liver loads were determined by real-time imaging of luciferase expressing parasites in livers of live mice 44 hours after ID sporozoite injection. We did not observe a difference in parasite liver load between mice infected with $Cy5M_2$-labeled sporozoites and mice infected with mock stained controls (5,6 ± 0,31 versus 5.7 ± 0,25 mean Log10 relative light units (RLU) respectively, p=0.18; Figure 4C). We tested $Cy5M_2$ concentrations of 50nM to 2.6uM, which did not affect sporozoite infectivity in HUH7 cells nor in mice (Figure 4A, Supplementary figure S6). The ability of $Cy5M_2$-labeled sporozoites to develop into blood stage malaria was demonstrated by positive blood smears at day seven post injection (Figure 4D) The prepatency of mice infected with $Cy5M_2$ labelled sporozoites was comparable to that of mice infected with unlabeled parasites, both at 6-7 days post infection.

Imaging of migration of $Cy5M_2$ labelled sporozoites in a human skin explant model

Since the aim of the development of a tracer labelling technique was to realize tracking of individual non-GMO sporozoites in human skin, we studied the migratory behavior of *in vitro* $Cy5M_2$-labelled non-GMO *Pf* sporozoites in human skin by confocal microscopy. (Figure 5A; movie S1). Using our custom analysis tool SMOOThuman skin (Sporozoite Motility Orienting and Organizing Tool) it was possible to isolate individual *Pf* sporozoites based on their $Cy5M_2$ fluorescent signature, and to record their migration over time. We generated 10 movies during which we were able to visualize 310 individual $Cy5M_2$ labelled non-GMO sporozoite tracks. 265 of imaged sporozoites were motile (85.5%) and allowed for segmentation of distinct movement patterns: sharp turns (39%), slight turns (13%) and linear movement (48%) (Figure 5B and C). Additionally, we were able to analyze the velocity of individual sporozoites over the full duration of their tracks (Figure 5D) or within individual movement pattern (Figure 5E). The latter revealed that linear segments displayed the highest velocity (median 0.86 μm/s) and velocity decreases with increased turning behavior (median 0.43 μm/s for slight turn and 0.29 μm/s for sharp turn, p=<0.0001; Figure 5E). Next to these motility characteristics, SMOOThuman skin extracts parameters of track tortuosity e.g. straightness index and angular dispersion (Supplementary figure S7). Taken together, these data demonstrate the potential of our custom tracer in imaging and analyzing non-GMO sporozoites in human skin.
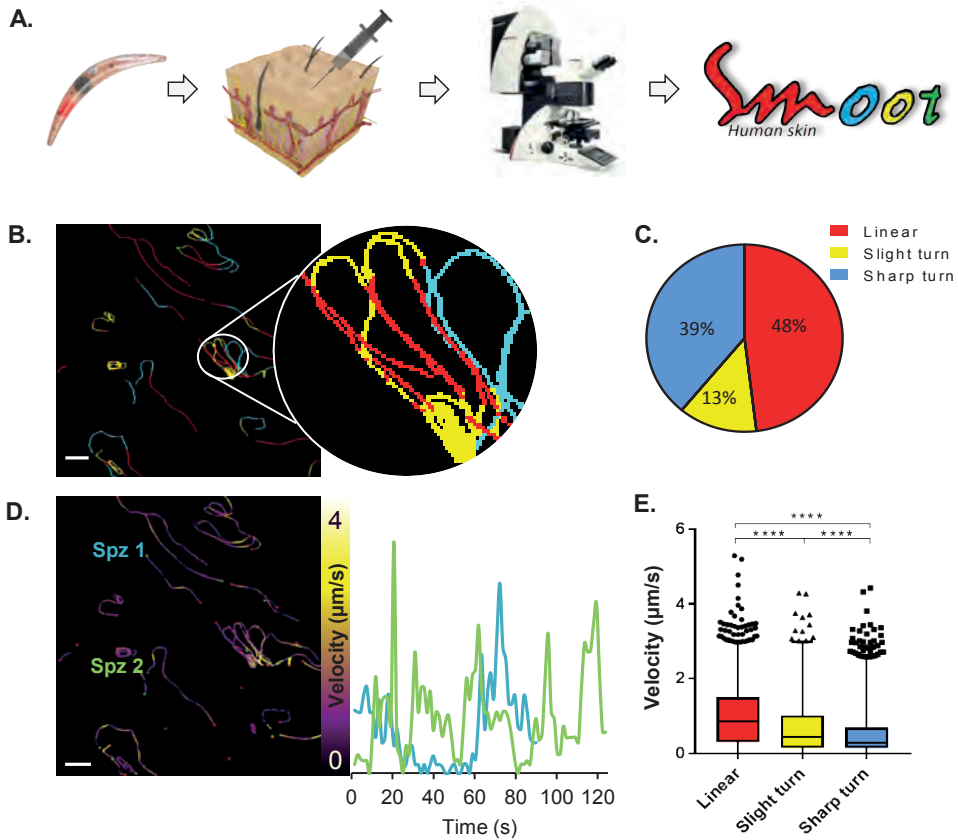
Figure 5. Labelled sporozoites can be tracked in a human skin explant model. (**A**) Non-GMO *Pf* sporozoites, *in vitro* labelled with Cy5M$_2$ are injected into human skin explants. Sliced punch biopsies are imaged using confocal microscopy. 2D video microscopy images are analyzed using SMOOT$_{human\ skin}$. (**B**) Individual sporozoites tracks visualized by migration pattern (linear in red, sharp turn in yellow slight turn in blue) and quantification of patterns (**C**). Velocity is tracked (**D**) and quantified (**E**) over the full duration of the track. ****: p=<0.0001 using one way analysis of variance (ANOVA) test.

DISCUSSION

Here we present a novel method to label live sporozoites using a mitochondrion-targeting labelling technique. This method allowed us to perform molecular imaging of non-GMO *Pf* in human skin and quantitatively analyze their motility. Uniquely, the Cy5M2 tracer could be universally applied to the *Plasmodium* species *Pb*, *Py* and *Pf*, and could be utilized to efficiently label sporozoites *in vitro* or to directly label sporozoites within the salivary glands of live mosquitoes. Subsequently, the labelling approach

allowed for cell-tracking of sporozoites. With that, a valuable step has been made towards the realization of *Pf* sporozoite imaging in human skin. We are convinced the application of the Cy5M$_2$ as a tool for imaging malaria sporozoites is of importance to the development of vaccines consisting of live-attenuated sporozoites.

There is a desperate need for tools that help unravel the mechanism of immune protection induced by malaria vaccine candidates. Antibody binding of sporozoites is likely to be an important effector mechanism after immunization with attenuated sporozoites[8,34,35] and results in altered motility of sporozoites under antibody attack[36,37]. Additionally, the recently EMA-approved malaria vaccine Mosquirix™ targets the highly abundant circumsporozoite protein (CSP) on the outer membrane of sporozoites and is associated with elevated anti-CSP antibody titres[34,38,39]. Despite this, the role of anti-CSP antibodies in the overall immune response against malaria remains controversial. For example, it is unknown what the relative contribution of these antibodies is in either blocking sporozoite migration from the skin to the blood or in blocking invasion of hepatocytes[35,37]. By allowing molecular-imaging based cell-tracking, the sporozoite-tracking technology presented in this study opens up novel possibilities on functional assays that study the effect that anti CSP antibodies (or antibodies against other sporozoite proteins) exert on sporozoite migration in human skin. Such studies may reveal pathways that support the development of new strategies that prevent infection.

To utilize molecular imaging to investigate the skin migratory behavior of *Plasmodium* sporozoites in humans, a highly expressed biomarker is required that can be targeted with a clinically acceptable tracer design. One of the prominent biomarkers in viable cells is mitochondrial metabolism. Therefore, we explored the use of the single mitochondrion in sporozoites as molecular target for *Plasmodium* sporozoite labelling. This targeting was verified through co-localization with MitoTracker® green. A competition assay with the known TSPO inhibitor PK11195 indicated that our mitochondrial dye Cy5M$_2$ targets a *Plasmodium* ortholog of TSPO. Uniquely, the presence of TSPO has not been previously been annotated in the *Plasmodium* genome. That said, the presence of TSPO analogues is considered universal in eukaryotic as well as prokaryotic cells[40-42]. It thus seems likely that *Plasmodium* mitochondria are equipped with a structure resembling mammalian TSPO, or at least a structure that binds similar ligands. This assumption is in line with reports that indicate TSPO inhibition affects blood stages of *Plasmodium* species *in vitro*[43,44]. A wide range of cell permeable small molecule benzodiazepine-, isoquinoline-, and pyrimidine-analogues have been reported to bind to TSPO19 and because TSPO is widespread in many cell types across species, some of these compounds have already been successfully translated to molecular imaging applications[45]. The same may become true for Cy5M$_2$, which may also be used to e.g. track different cell types.

The Cy5M$_2$ labelling technology enabled us to target more than 90% of all sporozoites within the mosquito and *in vitro* whereby 100% of all sporozoites were efficiently labelled. *In vitro* labelling was approximately 15 times more efficient compared to labelling within the mosquito. Flow cytometric analysis of *in vitro* labelled sporozoites identified only a small percentage (8.47%) of sporozoites exhibiting decreased staining efficiency. Whether the differences in Cy5M$_2$ staining within sporozoites reflect functional differences for example in infectivity or migrating potential, will be the subject of further studies. Interestingly, the decreased staining efficiency might be the result of different factors, such as the presence of transporters[46-49].

Our fitness assays did not reveal any evidence for toxicity of Cy5M$_2$ to sporozoites at the dose used. When extrapolating the current data for future use of Cy5M$_2$-labelled sporozoites in humans, we expect Cy5M$_2$ toxicity to the human host to be negligible. Reasoning that even if all Cy5M$_2$ is taken up during *in vitro* labelling of 106 *Pf* sporozoites (2.6uM in 1 ml), this would result in a total maximum dose of 1ug Cy5M$_2$ or (1pg per sporozoite). At this dose, toxicity assessments of this compound would fall within the tracer dose regime, a property that supports the translational nature of the presented labelling technology[50,51]. Obviously, when increased understanding of the in human behavior of *Pf* sporozoites allows for the doses of attenuated sporozoites to be lowered, overall toxicity risk decreases even further.

Our quantitative assessment of migrating *Pf* sporozoites in human skin underlines the potential of this new cell-tracking technology for imaging of non-GMO *Pf* sporozoites in the human skin to study factors and mechanisms influencing host-to-host transmission. Using our custom SMOOT$_{\text{human skin}}$ software we were able to extract dermal migration behavior data from individual non-GMO *Pf* sporozoites both in detail and over time. Our data show highly directional movement patterns of migrating sporozoites, as well as high velocity variability within sporozoite tracks. Velocity correlated with movement pattern, with parasites slowing down as their tortuosity increased. Variations in velocity and/or movement pattern may correspond with sporozoite interactions with the tissue environment and may therefore indicate sites of particular interest[5,52].

With the presented technology we have been able to study sporozoite behavior skin deep. To extend the use of this technology for imaging beyond the skin stage, a matching nuclear medicine-based imaging approach, or preferably a hybrid imaging approach will have to be developed[53]. Increased signal intensity per sporozoite through potentiated mitochondrial targeting, may be realized with the use of recent chemical developments in the area of nanotechnology[54]. Such developments will facilitate

further use in malaria research, where imaging of small numbers of parasites will help to elucidate the mystery of non-hepatic development of sporozoites and lymph node trafficking, analogous to experiments with *Pb* in rodents[13].

Conclusion

We have implemented a fluorescence-based molecular imaging approach based on an exogenous fluorescent tracer that allows direct imaging of *Plasmodium* sporozoites in human tissue. Uniquely, the Cy5M$_2$ labelling approach is a universally applicable technology which even permits labelling of *Plasmodium* sporozoites while still residing in the live mosquito host. This initial study demonstrated that this technology has the potential to help unravel the fundamental features of skin migration of malaria parasites in humans. Molecular imaging of sporozoite migration in humans allows investigation of factors and mechanisms influencing host-to-host transmission, knowledge that is essential for further development of highly effective vaccines targeting the sporozoite stage.

SUPPLEMENTARY NOTES

Author contribution statement: BW, MO,DS, AB, ML, BF, SC and CK performed the experiments. BW, MO, CK, CJ, FvL and MR interpreted the data. BW, FvL and MR drafted the manuscript. All authors reviewed and contributed to finalizing the manuscript.

Ethics statement: The use of human skin explants (obtained as waste material after abdominal reduction surgery) for this research was approved by the Commission Medical Ethics (CME) of the LUMC, Leiden. Approval number CME: B18-009.

Competing interests: The authors declare no competing financial interests.

REFERENCES

1   [Internet] WHO: Geneva Switzerland. 19 November 2018, World Malaria report 2018. https://www.who.int/malaria/media/world-malaria-report-2018/en/.

2   Medica, D. L. & Sinnis, P. Quantitative dynamics of Plasmodium yoelii sporozoite transmission by infected anopheline mosquitoes. Infect Immun 73, 4363-4369, doi:10.1128/IAI.73.7.4363-4369.2005 (2005).

3   Sack, B. K. et al. Model for in vivo assessment of humoral protection against malaria sporozoite challenge by passive transfer of monoclonal antibodies and immune serum. Infect Immun 82, 808-817, doi:10.1128/IAI.01249-13 (2014).

4   Vanderberg, J. P. & Frevert, U. Intravital microscopy demonstrating antibody-mediated immobilisation of Plasmodium berghei sporozoites injected into skin by mosquitoes. Int J Parasitol 34, 991-996, doi:10.1016/j.ijpara.2004.05.005 (2004).

5   Amino, R. et al. Quantitative imaging of Plasmodium transmission from mosquito to mammal. Nat Med 12, 220-224, doi:10.1038/nm1350 (2006).

6   Roestenberg, M. et al. Protection against a malaria challenge by sporozoite inoculation. N Engl J Med 361, 468-477, doi:10.1056/NEJMoa0805832 (2009).

7   Epstein, J. E. et al. Live attenuated malaria vaccine designed to protect through hepatic CD8(+) T cell immunity. Science 334, 475-480, doi:10.1126/science.1211548 (2011).

8   Bastiaens, G. J. et al. Safety, Immunogenicity, and Protective Efficacy of Intradermal Immunization with Aseptic, Purified, Cryopreserved Plasmodium falciparum Sporozoites in Volunteers Under Chloroquine Prophylaxis: A Randomized Controlled Trial. Am J Trop Med Hyg 94, 663-673, doi:10.4269/ajtmh.15-0621 (2016).

9   Haeberlein, S. et al. Protective immunity differs between routes of administration of attenuated malaria parasites independent of parasite liver load. Sci Rep 7, 10372, doi:10.1038/s41598-017-10480-1 (2017).

10   Seder, R. A. et al. Protection against malaria by intravenous immunization with a nonreplicating sporozoite vaccine. Science 341, 1359-1365, doi:10.1126/science.1241800 (2013).

11   Hopp, C. S. et al. Longitudinal analysis of Plasmodium sporozoite motility in the dermis reveals component of blood vessel recognition. Elife 4, doi:10.7554/eLife.07789 (2015).

12   Yamauchi, L. M., Coppi, A., Snounou, G. & Sinnis, P. Plasmodium sporozoites trickle out of the injection site. Cell Microbiol 9, 1215-1222, doi:10.1111/j.1462-5822.2006.00861.x (2007).

13   Gueirard, P. et al. Development of the malaria parasite in the skin of the mammalian host. Proc Natl Acad Sci U S A 107, 18640-18645, doi:10.1073/pnas.1009346107 (2010).

14   da Silva, H. B. et al. Early skin immunological disturbance after Plasmodium-infected mosquito bites. Cell Immunol 277, 22-32, doi:10.1016/j.cellimm.2012.06.003 (2012).

15   Mac-Daniel, L. et al. Local immune response to injection of Plasmodium sporozoites into the skin. J Immunol 193, 1246-1257, doi:10.4049/jimmunol.1302669 (2014).

16   Massoud, T. F. & Gambhir, S. S. Molecular imaging in living subjects: seeing fundamental biological processes in a new light. Genes Dev 17, 545-580, doi:10.1101/gad.1047403 (2003).

17   Bunschoten, A., Welling, M. M., Termaat, M. F., Sathekge, M. & van Leeuwen, F. W. Development and prospects of dedicated tracers for the molecular imaging of bacterial infections. Bioconjug Chem 24, 1971-1989, doi:10.1021/bc4003037 (2013).

18   van den Berg, N. S. et al. Multimodal Surgical Guidance during Sentinel Node Biopsy for

Melanoma: Combined Gamma Tracing and Fluorescence Imaging of the Sentinel Node through Use of the Hybrid Tracer Indocyanine Green-(99m)Tc-Nanocolloid. Radiology 275, 521-529, doi:10.1148/radiol.14140322 (2015).

19   Rupprecht, R. et al. Translocator protein (18 kDa) (TSPO) as a therapeutic target for neurological and psychiatric disorders. Nat Rev Drug Discov 9, 971-988, doi:10.1038/nrd3295 (2010).

20   Li, F. et al. Translocator Protein 18 kDa (TSPO): An Old Protein with New Functions? Biochemistry 55, 2821-2831, doi:10.1021/acs.biochem.6b00142 (2016).

21   Hatty, C. R. & Banati, R. B. Protein-ligand and membrane-ligand interactions in pharmacology: the case of the translocator protein (TSPO). Pharmacol Res 100, 58-63, doi:10.1016/j.phrs.2015.07.029 (2015).

22   Otto, T. D. et al. A comprehensive evaluation of rodent malaria parasite genomes and gene expression. BMC Biol 12, 86, doi:10.1186/s12915-014-0086-0 (2014).

23   Prado, M. et al. Long-term live imaging reveals cytosolic immune responses of host hepatocytes against Plasmodium infection and parasite escape mechanisms. Autophagy 11, 1561-1579, doi:10.1080/15548627.2015.1067361 (2015).

24   Kooij, T. W., Rauch, M. M. & Matuschewski, K. Expansion of experimental genetics approaches for Plasmodium berghei with versatile transfection vectors. Mol Biochem Parasitol 185, 19-26, doi:10.1016/j.molbiopara.2012.06.001 (2012).

25   Lin, J. W. et al. A novel 'gene insertion/marker out' (GIMO) method for transgene expression and gene complementation in rodent malaria parasites. PLoS One 6, e29289, doi:10.1371/journal.pone.0029289 (2011).

26   Sinden, R. E. Infection of mosquitoes with rodent malaria. The Molecular Biology of Insect Disease Vectors: a Methods Manual (ed. J. M. Crampton, C. B. Beard and C. Louis), pp. 67-91 (1997).

27   Ponnudurai, T., Leeuwenberg, A. D. & Meuwissen, J. H. Chloroquine sensitivity of isolates of Plasmodium falciparum adapted to in vitro culture. Trop Geogr Med 33, 50-54 (1981).

28   Ponnudurai, T. et al. Infectivity of cultured Plasmodium falciparum gametocytes to mosquitoes. Parasitology 98 Pt 2, 165-173 (1989).

29   Fougere, A. et al. Variant Exported Blood-Stage Proteins Encoded by Plasmodium Multigene Families Are Expressed in Liver Stages Where They Are Exported into the Parasitophorous Vacuole. PLoS Pathog 12, e1005917, doi:10.1371/journal.ppat.1005917 (2016).

30   Rougemont, M. et al. Detection of four Plasmodium species in blood from humans by 18S rRNA gene subunit-based and species-specific real-time PCR assays. J Clin Microbiol 42, 5636-5643, doi:10.1128/JCM.42.12.5636-5643.2004 (2004).

31   van der Velden, M. et al. Protective Efficacy Induced by Genetically Attenuated Mid-to-Late Liver-Stage Arresting Plasmodium berghei Deltamrp2 Parasites. Am J Trop Med Hyg 95, 378-382, doi:10.4269/ajtmh.16-0226 (2016).

32   De Niz, M. et al. Progress in imaging methods: insights gained into Plasmodium biology. Nat Rev Microbiol 15, 37-54, doi:10.1038/nrmicro.2016.158 (2017).

33   Sturm, A., Mollard, V., Cozijnsen, A., Goodman, C. D. & McFadden, G. I. Mitochondrial ATP synthase is dispensable in blood-stage Plasmodium berghei rodent malaria but essential in the mosquito phase. Proc Natl Acad Sci U S A 112, 10216-10223, doi:10.1073/pnas.1423959112 (2015).

34   Ishizuka, A. S. et al. Protection against malaria at 1 year and immune correlates following PfSPZ vaccination. Nat Med 22, 614-623, doi:10.1038/nm.4110 (2016).

35   Flores-Garcia, Y. et al. Antibody-Mediated Protection against Plasmodium Sporozoites

Begins at the Dermal Inoculation Site. MBio 9, doi:10.1128/mBio.02194-18 (2018).

36   Stewart, M. J., Nawrot, R. J., Schulman, S. & Vanderberg, J. P. Plasmodium berghei sporozoite invasion is blocked in vitro by sporozoite-immobilizing antibodies. Infect Immun 51, 859-864 (1986).

37   Aliprandini, E. et al. Cytotoxic anti-circumsporozoite antibodies target malaria sporozoites in the host skin. Nat Microbiol 3, 1224-1233, doi:10.1038/s41564-018-0254-z (2018).

38   Casares, S., Brumeanu, T. D. & Richie, T. L. The RTS,S malaria vaccine. Vaccine 28, 4880-4894, doi:10.1016/j.vaccine.2010.05.033 (2010).

39   Cohen, J., Nussenzweig, V., Nussenzweig, R., Vekemans, J. & Leach, A. From the circumsporozoite protein to the RTS, S/AS candidate vaccine. Hum Vaccin 6, 90-96 (2010).

40   Yeliseev, A. A. & Kaplan, S. A sensory transducer homologous to the mammalian peripheral-type benzodiazepine receptor regulates photosynthetic membrane complex formation in Rhodobacter sphaeroides 2.4.1. J Biol Chem 270, 21167-21175 (1995).

41   Chapalain, A. et al. Bacterial ortholog of mammalian translocator protein (TSPO) with virulence regulating activity. PLoS One 4, e6096, doi:10.1371/journal.pone.0006096 (2009).

42   Papadopoulos, V. et al. Translocator protein (18kDa): new nomenclature for the peripheral-type benzodiazepine receptor based on its structure and molecular function. Trends Pharmacol Sci 27, 402-409, doi:10.1016/j.tips.2006.06.005 (2006).

43   Marginedas-Freixa, I. et al. TSPO ligands stimulate ZnPPIX transport and ROS accumulation leading to the inhibition of P. falciparum growth in human blood. Sci Rep 6, 33516, doi:10.1038/srep33516 (2016).

44   Dzierszinski, F. et al. Ligands of the peripheral benzodiazepine receptor are potent inhibitors of Plasmodium falciparum and Toxoplasma gondii in vitro. Antimicrob Agents Chemother 46, 3197-3207 (2002).

45   Vivash, L. & O'Brien, T. J. Imaging Microglial Activation with TSPO PET: Lighting Up Neurologic Diseases? J Nucl Med 57, 165-168, doi:10.2967/jnumed.114.141713 (2016).

46   Koenderink, J. B., Kavishe, R. A., Rijpma, S. R. & Russel, F. G. The ABCs of multidrug resistance in malaria. Trends Parasitol 26, 440-446, doi:10.1016/j.pt.2010.05.002 (2010).

47   Wongsrichanalai, C., Pickard, A. L., Wernsdorfer, W. H. & Meshnick, S. R. Epidemiology of drug-resistant malaria. Lancet Infect Dis 2, 209-218 (2002).

48   Rijpma, S. R. et al. Multidrug ATP-binding cassette transporters are essential for hepatic development of Plasmodium sporozoites. Cell Microbiol 18, 369-383, doi:10.1111/cmi.12517 (2016).

49   Mu, J. et al. Multiple transporters associated with malaria parasite responses to chloroquine and quinine. Mol Microbiol 49, 977-989 (2003).

50   KleinJan, G. H. et al. Fluorescence guided surgery and tracer-dose, fact or fiction? Eur J Nucl Med Mol Imaging 43, 1857-1867, doi:10.1007/s00259-016-3372-y (2016).

51   [internet] European Medicines Agency EMA. 2018, http://www.ema.europa.eu/ema.

52   Battista, A., Frischknecht, F. & Schwarz, U. S. Geometrical model for malaria parasite migration in structured environments. Phys Rev E Stat Nonlin Soft Matter Phys 90, 042720, doi:10.1103/PhysRevE.90.042720 (2014).

53   KleinJan, G. H. et al. Multimodal imaging in radioguided surgery. Clin Transl Imaging 1, 433-444 (2013).

54   Lynn E. Samuelson, B. M. A., Mingfeng Bai, Madeline J Dukes,, Colette R. Hunt, J. D. C., Zeqiu Han, Vassilios Papadopoulosc & Bornhop, a. D. J. A self-internalizing mitochondrial TSPO targeting imaging probe for fluorescence, MRI and EM. RSC Adv. 4, 9003 (2014).

SUPPLEMENTARY INFORMATION

Methods

Synthesis of Cy5-methyl-methyl (Cy5M$_2$)

Indol-Methyl

In brief, 2,3,3-trimethylindolenine (25 mmol) and methyl iodide (30 mmol) were stirred in toluene (40 ml) for 16h at 40 °C. The formed suspension was filtered, and the precipitate was dried in vacuo yielding pink crystals (4 g) and used without further purification.

Cy5-Methyl-Methyl

Indol-Methyl (13.28 mmol), 3-anilinoacraldehyde (6.64 mmol) and sodium acetate (15.49 mmol) were stirred in ethanol absolute (150 ml) and refluxed for 8h under nitrogen atmosphere followed by stirring at room temperature for 6h. The mixture was concentrated and purified by silica gel chromatography using acetonitrile:methanol 3:1, followed by methanol, followed by methanol + 0.25%AcOH. After lyophilization a dark powder (148 mg) was obtained.
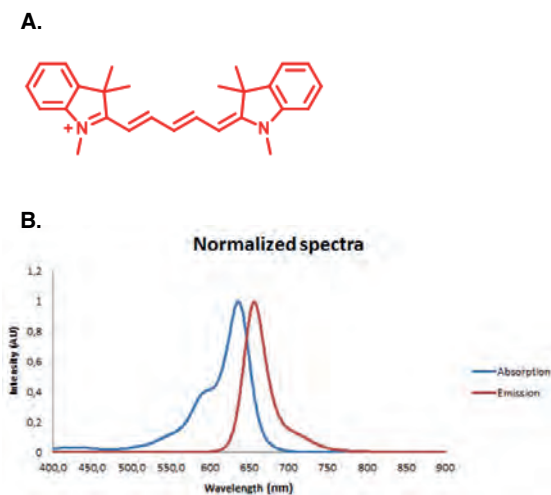
A.

B.

Figure S1. Properties of Cy5M$_2$. Molecular structure (**A**) and normalized absorption (blue) and emission spectra (red) of Cy5M$_2$ (**B**).

Cy5M$_2$ binding specificity for TSPO

Confocal microscopy

The binding specificity of Cy5M$_2$ was initially evaluated *in vitro* using two mammalian cell lines that have a higher mitochondrial density and thus TSPO expression levels than sporozoites: Human breast cancer cell line MDAMB213 X4 cells (X4-cells), kindly provided by Dr. G. Luker (University of Michigan, Ann Arbor, USA), wherein CXCR4 expression was acquired after transfection with a GFP-tagged version of the human CXCR4-gene[1] and RT4-D6P2T rat Schwannoma cell line (RT4-cells), obtained from ATCC (American Type Culture Collection, Manassas, VA, USA). Both cell lines were maintained in Dulbecco's modified Eagle medium (DMEM) enriched with 10% fetal bovine serum and 1% penicillin/streptomycin (all Life Technologies Inc. Carlsbad, CA, USA). Cells were kept under standard culture conditions. The cultured cells were trypsinized and seeded onto coverslips (ø35mm; MatTek Corporation) and incubated overnight in medium.

To validate the mitochondrial localization, Cy5M$_2$ was applied together with Mitotracker® green (Thermo Fisher Scientific, Waltham, MA, USA). RT-4 cells were incubated with 1 μM Mitotracker green® (for 1 hour at 37°C) before the incubation with Cy5M$_2$ (5 min at RT with 3nM). To confirm TSPO binding specificity of Cy5M$_2$, blocking experiments were performed with the known TSPO inhibitor PK11195[2] (Sigma Aldrich). Both RT4-cells and X4-cells were incubated with 50 μM PK11195 (40 minutes at 37°C), before the incubation with Cy5M$_2$ (5 min at room temperature (RT); 3nM). All samples were washed with PBS prior to confocal microscopy analysis (Leica TCS SP8X WLL microscope (Leica Microsystems, Wetzlar, Germany)). Cy5 was excited at 633 nm and the emission was collected between 650-700 nm, the laser power was kept constant during the comparative experiments.

SMOOT$_{human skin}$

MATLAB (The MathWorks Inc. Natick, MA, USA) software was created for in skin sporozoite analysis. Using this software, we were able to extract the following features per sporozoite over time: movement pattern, angular dispersion, straightness index and velocity. Sporozoite tracks were characterized as motile or stationary based on their displacement. Subsequently, the movement patterns: *sharp turn, slight turn* and *linear* were segmented from motile tracks.

Straightness index (SI)

The SI is a measurement for the deviation of a track from a straight line and is used to quantify track tortuosity. It is defined as the ratio of distance between track end point (*C*) and track length (*L*), as calculated using formula (1). e.g. SI = 1 in a perfect linear path, SI = 0 when the path describes a circle.

$$SI = \frac{C_{track}}{L_{track}} = \frac{x(i) - x(0)}{\sum_{k=1}^{i}(x(k) - x(k-1))} \tag{1}$$

Angular dispersion (AD)

The AD describes tortuosity by quantifying changes in direction by measuring deviation from the mean angle of movement. It is calculated according to the following formula:

$$AD = \frac{1}{I}\sqrt{C^2 + S^2} \tag{2}$$

Where *I* is the last step of the track and *C and S* are defined as:

$$C = \sum_{i=1}^{I} \cos \theta_i \qquad\qquad S = \sum_{i=1}^{I} \sin \theta_i$$

Where θ is the turn angle of the sporozoite track, defined by the angle difference between path directions in consecutive frames.

$$\theta_i = \delta_i - \delta_{i-1}$$

e.g. AD = 1 indicates a consistent angle (either a straight line or a perfect circle) and smaller AD values represent the presence of random turns over the track course.

Velocity

Sporozoite velocity was measured using the displacement between frames. We defined step number in the track *i* to measure velocity *v* using formula (3), with *x as* the median pixel location of the sporozoite and *t* as the time duration in seconds.

$$v(i) = \frac{x_i - x_{i-1}}{t_i - t_{i-1}} = \frac{dx}{dt} \tag{3}$$

Supplementary video 1 available on:
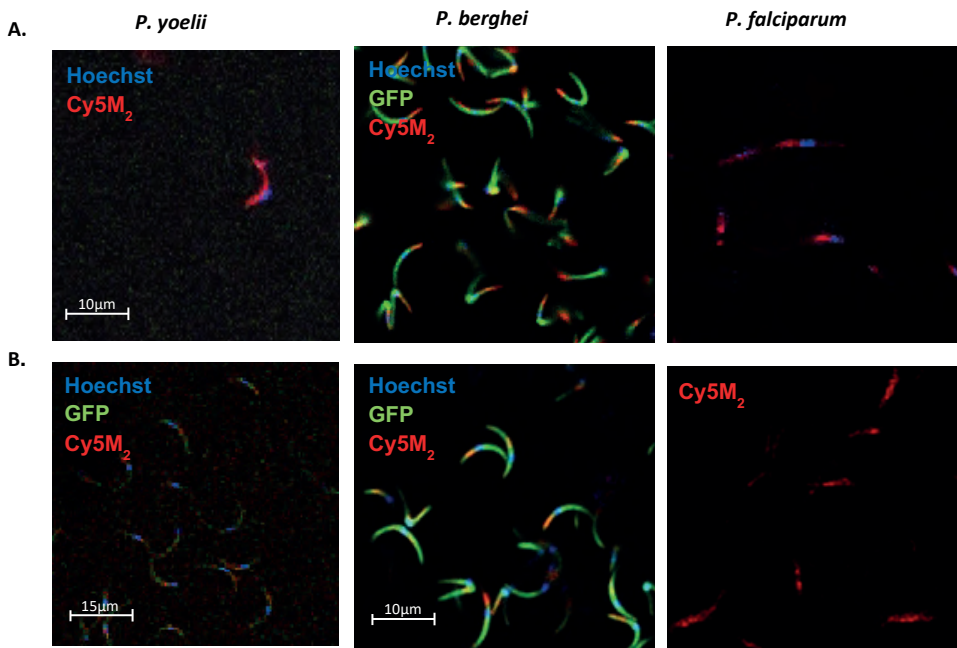https://www.thno.org/v09/p2768/thnov09p2768s2.mp4

Results

Figure S2. Cy5M$_2$ labels rodent and human malaria sporozoites. Labelling of different *Plasmodium* species with Cy5M$_2$, both *in vitro* (**A**, upper panels) as well as *in vivo* (**B**, lower panels) within the mosquito host. Overlay images of indicated colours. Brightfield in grey, Hoechst in blue, GFP in green and Cy5M$_2$ in red. Scale bar 10μM
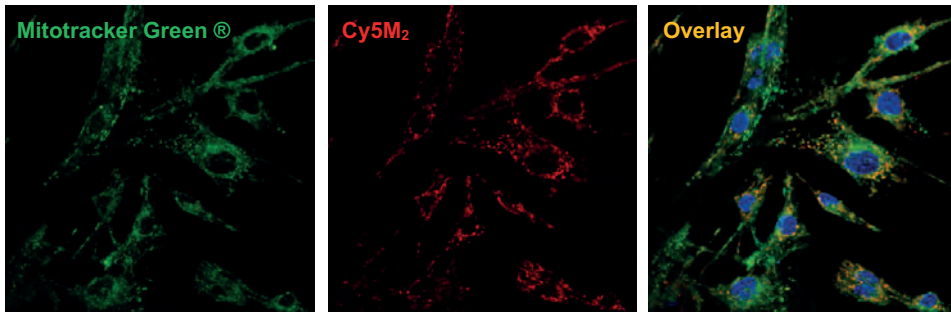
Figure S3. Co-localization of mitochondrial Cy5M$_2$ and MitoTracker® Green. RT4-cells were stained with Mitotracker® green (green) and Cy5M$_2$ (red). Nuclei are stained with Hoechst (blue). Scale bar 50μM.
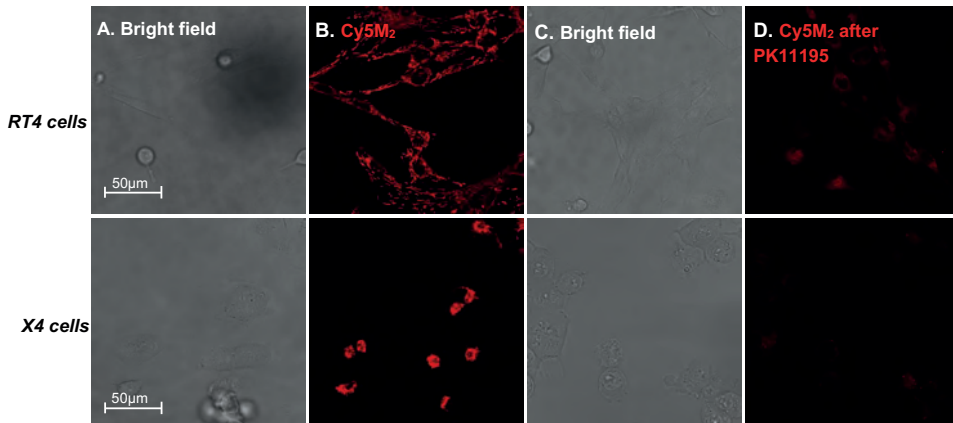

Figure S4. Competitive binding assay of Cy5M$_2$ with PK11195 in cell lines. A,B. RT4-cells (top panels) and X4-cells (bottom panels) are stained with Cy5M$_2$ (**r**ed). **C,D.** Cy5M$_2$ binding is blocked with PK11195.
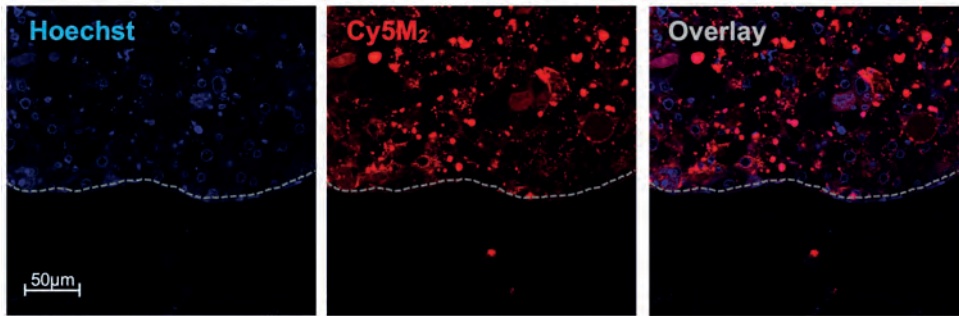
Figure S5. Cy5M$_2$ staining of the mosquito midgut. Midguts of *Pb* infected *Anopheles* mosquitoes fed on Cy5M$_2$. Mosquitoes were dissected 15 minutes after feeding. Midgut cells stained with Cy5M$_2$ (red), nuclei are stained with Hoechst (blue). Scale bar 50μM
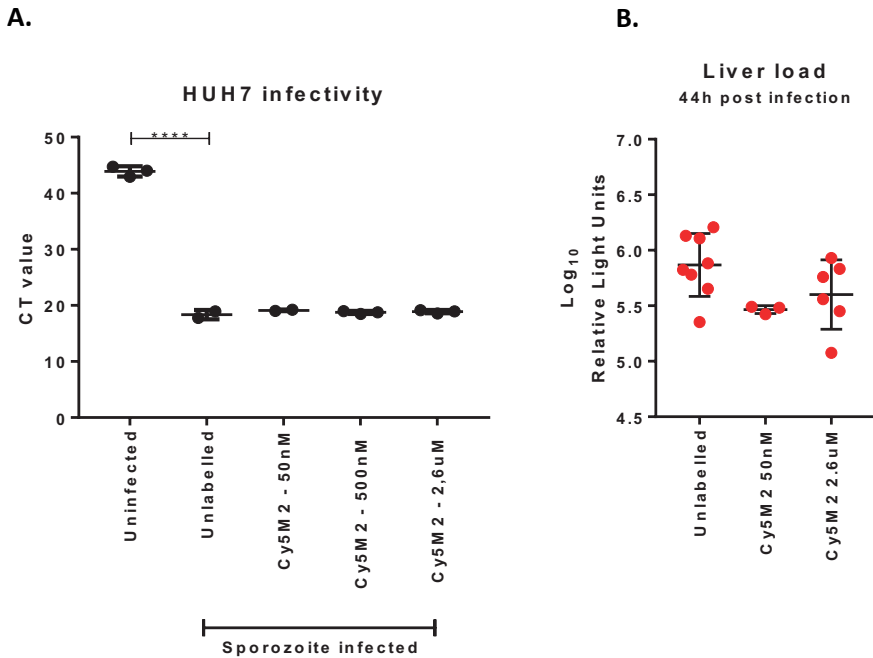

Figure S6. Sporozoite infectivity after Cy5M$_2$ labelling. Sporozoite infectivity in HUH7 hepatoma cells (**A**) or in mice (**B**) was not affected by increased dosages of Cy5M$_2$. **A.** PCR data showing similar levels of HUH7 cell infection with all dosages of Cy5M$_2$ labelled sporozoites compared to unlabeled controls. **B**. Quantification of liver load measured by IVIS 44h post infection Cumulative results from 2 separate experiments (n=8 unlabelled; n=3 TCy5M$_2$ 50μM and n=8 Cy5M$_2$ 2,6μM). Statistical analysis: Student's T test. ****= p<0,0001

A.

Straightness index (SI)

B.

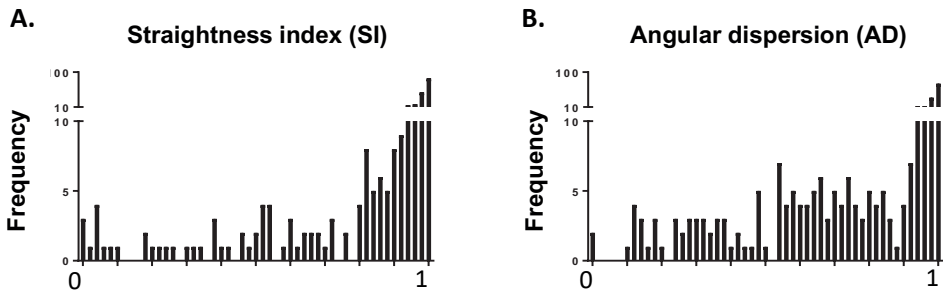### Angular dispersion (AD)

Figure S7. Tortuosity *Pf* tracks in human skin. The tortuosity of sporozoite tracks is quantified using the Straightness index (SI; **A**) and Angular dispersion (AD; **B**). The SI was non-parametrically distributed with the majority of tracks displaying high values (relatively straight tracks; median SI 0.97). Track AD values showed three peaks, indicating three subgroups of tracks. The majority of tracks had a high AD, indicating consistent directions of movement, as opposed to random variations.

REFERENCES

1   Luker, K. E., Gupta, M., & Luker, G. D. Bioluminescent CXCL12 fusion protein for cellular studies of CXCR4 and CXCR7. BioTechniques. 2009; 47: 625-632

2   Hatty, C. R., & Banati, R. B. Protein-ligand and membrane-ligand interactions in pharmacology: the case of the translocator protein (TSPO). Pharmacological Research. 2015; 100, 58-63.